Superelastic and Superhydrophobic Nanofiber-Assembled Cellular Aerogels for Effective Separation of Oil/Water Emulsions

Yang Si,[†,‡] Qiuxia Fu,[†] Xueqin Wang,[‡] Jie Zhu,[†] Jianyong Yu,[†,§] Gang Sun,[†,§] and Bin Ding*[,†,‡]

[†]Key Laboratory of Textile Science & Technology, Ministry of Education, College of Textiles, Donghua University, Shanghai 201620, China, [‡]State Key Laboratory for Modification of Chemical Fibers and Polymer Materials, College of Materials Science and Engineering, Donghua University, Shanghai 201620, China, and [§]Nanomaterials Research Center, Modern Textile Institute, Donghua University, Shanghai 200051, China

ABSTRACT Many applications proposed for functional nanofibers require their assembly into a monolithic cellular structure. The ability to maintain structural integrity upon large deformation is essential to ensure a macroscopic cellular material that functions reliably. However, it remains a great challenge to achieve high elasticity in three-dimensional (3D) nanofibrous networks. Here, we report a strategy to create fibrous, isotropically bonded elastic reconstructed (FIBER) aerogels with a hierarchical cellular structure and superelasticity by combining electrospun nanofibers and the freeze-shaping technique. Our approach allows the intrinsically lamellar deposited electrospun nanofibers to assemble into elastic bulk aerogels with tunable porous structure and wettability on a large scale. The resulting FIBER aerogels exhibit the integrated properties of ultralow density (<30 mg cm^{-3}), rapid recovery from 80% compression strain, superhydrophobic-superoleophilic wettability, and high pore tortuosity. More interestingly, the FIBER aerogels can effectively separate surfactant-stabilized water-in-oil emulsions, solely using gravity, with high flux (maximum of 8140 $\pm$ 220 L m^{-2} h^{-1}) and high separation efficiency, which match well with the requirements for treating the real emulsions. The synthesis of FIBER aerogels also provides a versatile platform for exploring the applications of nanofibers in a self-supporting, structurally adaptive, and 3D macroscopic form.

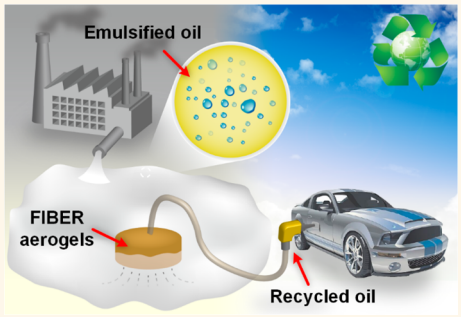

KEYWORDS: aerogels · nanofibers · superelastic · superhydrophobic · emulsion separation

Oil/water separation is a worldwide challenge due to the ever-increasing industrial oily wastewater and polluted oceanic waters, as well as frequent oil spill accidents such as the Deepwater Horizon oil spill in the Gulf of Mexico.[1−3] Conventional methods such as oil skimmers, centrifuges, depth filters, sedimentation, and flotation are useful for separation of immiscible oil/water mixtures, but are not effective for emulsified oil/water mixtures, especially not for microemulsions (droplet sizes <20 μm) with the presence of surfactants.[4,5] Membrane-based technologies, such as ultrafiltration (UF), which selectively allows materials of certain sizes to pass through the membrane pores on the basis of the size-sieving effect, have been successfully applied to separate various industrial emulsions.[6−8] However, these pressure-driven separation membranes generally suffer from low flux and energy consumption due to small pore size (<0.3 μm). The two-dimensional membrane structure with low porosity and short permeation channels usually causes serious fouling and degradation because of surfactant adsorption and pore plugging, which lead to a quick decline of the separation performance.[8−10] Alternatively, three-dimensional (3D) bulk aerogels are known to possess versatile porosity, low density, and high internal surface area properties, as well as easily be used to make monolithic solids of desired shapes.[11,12] Therefore, creating functional aerogels with special wettability and tortuously porous structure could be another strategy for realizing promising separation performance as demulsification is achieved. Several functional

* Address correspondence to binding@dhu.edu.cn.

Received for review November 20, 2014 and accepted April 8, 2015.

Published online April 08, 2015
10.1021/nn506633b

aerogels such as silica colloid aerogels, carbon nanotube aerogels, graphene monoliths, porous boron nitride, and polymer sponges have recently been applied to oil–water separation.[13−17] However, previous efforts mainly used these aerogels as oil absorbents and focused excessively on the oil absorption capacity, ignoring the time-consuming and cost oil recovery procedures by squeezing or distillation. The challenge, therefore, is to construct a porous, special wetted, and mechanically robust aerogel capable of efficient, cost-effective separation of oil/water emulsions, especially in a direct, continuous, and self-driving way.

The systematic design of aerogels for oil/water emulsion separation requires the optimization of two important characteristics: surface wettability, which affects the interception and demulsification of the emulsified liquid droplets, and the cellular structure, which dictates the permeation rate of one phase (for example, oil) pass through the aerogels.[18−21] Electrospun nanofibers, as the forefront of advanced fibrous materials, combine the tunable wettability, good connectivity, robust mechanical strength, fine flexibility, large surface area, and ease of scalable synthesis from various materials (polymer, ceramic, carbon, *etc.*), hold great promise as exceptional nanoscale building blocks for constructing functional aerogels.[22−24] Despite their outstanding potential, no effort has been made to use electrospun nanofibers for the preparation of aerogels for emulsion separation. The major problem associated with electrospun nanofibers is their anisotropic lamellar deposition character, with the resultant nanofibers usually assembling into close-packed membranes (with thicknesses <100 μm) rather than into bulk aerogels.[25,26] This issue has never been systematically addressed before.

In this work, we present a robust methodology for creating superelastic and superhydrophobic aerogels with a hierarchical cellular structure that consists of bonded nanofibers, which we call "fibrous, isotropically-bonded elastic reconstructed" (FIBER) aerogels. The premise for our design is that the intrinsically lamellar deposited electrospun nanofibers are reconstructed into 3D fibrous bulk aerogels with tunable porous structure and wettability on a large scale. Our FIBER aerogels exhibit the integrated properties of ultralow density, super recyclable compressibility, superhydrophobic-superoleophilic wettability, and high pore tortuosity, which can effectively separate surfactant-stabilized water-in-oil emulsions, solely using gravity, with a high flux that is several times higher than that of commercial filtration membranes driven by external pressure. We also demonstrate an oil recycling apparatus based on a simple combination of FIBER aerogels and a peristaltic pump to realize continuous collection of oil *in situ* from the oil/water emulsions with high speed and efficiency.

RESULTS AND DISCUSSION

We designed the FIBER aerogels based on three criteria: (1) the nanofibers must assemble into a 3D aerogel with an open-cell cellular architecture rather than into a membrane, (2) the aerogels must be mechanically robust and resistant to fatigue upon compressive deformation, and (3) the water-in-oil emulsions must be completely demulsified and separated as they move through the aerogels. The first requirement was satisfied by a versatile, readily accessible, and gelation-free fibrous freeze-shaping method, which involved the homogenization of nanofibers, the freeze-drying assembly, and the final *in situ* cross-linking. Figure 1a describes the synthesis pathway. Polyacrylonitrile (PAN) and SiO_2 nanofibers were selected as the major building blocks to construct the hybrid fibrous networks (Figure S1, Supporting Information), and the SiO_2 nanoparticles (SiO_2 NPs) were introduced into aerogels to enhance the porous structure. A low surface energy fluoric bifunctional benzoxazine (BAF-a) was used as a novel *in situ* cross-linking agent (Figure S2a). The as-prepared PAN and SiO_2 electrospun nanofiber membranes were first homogenized in camphene at 70 °C to form a well-dispersed nanofiber dispersion, then the SiO_2 NPs (various concentrations of 0, 0.01, 0.1, 0.5, 1, and 2 wt %) and BAF-a (0.5 wt %) were added to the dispersion with further stirring. Following, the dispersion was freeze-dried into unbonded aerogels (see details in Figure S3 and S4).

The initial freeze-dried unbonded aerogels were fragile toward external stress. To satisfy the second criterion—the formation of mechanically robust fibrous networks—the obtained unbonded aerogels were heated at 240 °C for 1 h to form bonded 3D fibrous networks, endowing the resultant FIBER aerogels with elastic resilience (Figure S5). The principle of bonding process was based on the *in situ* polymerization of the BAF-a monomers on the fiber surface, which led to the formation of Mannich-bridged PBZ, and cemented the adjacent nanofibers.[27,28] Simultaneously, the thermoplastic PAN fibers were also converted into stable and elastic ladder-structured PAN *via* cyclization reaction.[29] Fourier transform infrared (FT-IR) spectra and differential scanning calorimetry (DSC) analyses have proven the formation of cyclized PAN and PBZ. (see Figure S6 and Supporting Information Discussions). In addition, the PAN nanofibers tended to generate dramatic heat shrinkage along their long axes due to the relaxation of oriented molecular chains,[30] whereas the thermally stable SiO_2 nanofibers in aerogels acted as a rigid support to prevent the fibrous networks from collapsing. We found that the FIBER aerogels with stable shape and structure can be achieved by adding 20 wt % SiO_2 nanofibers (Figure S7).

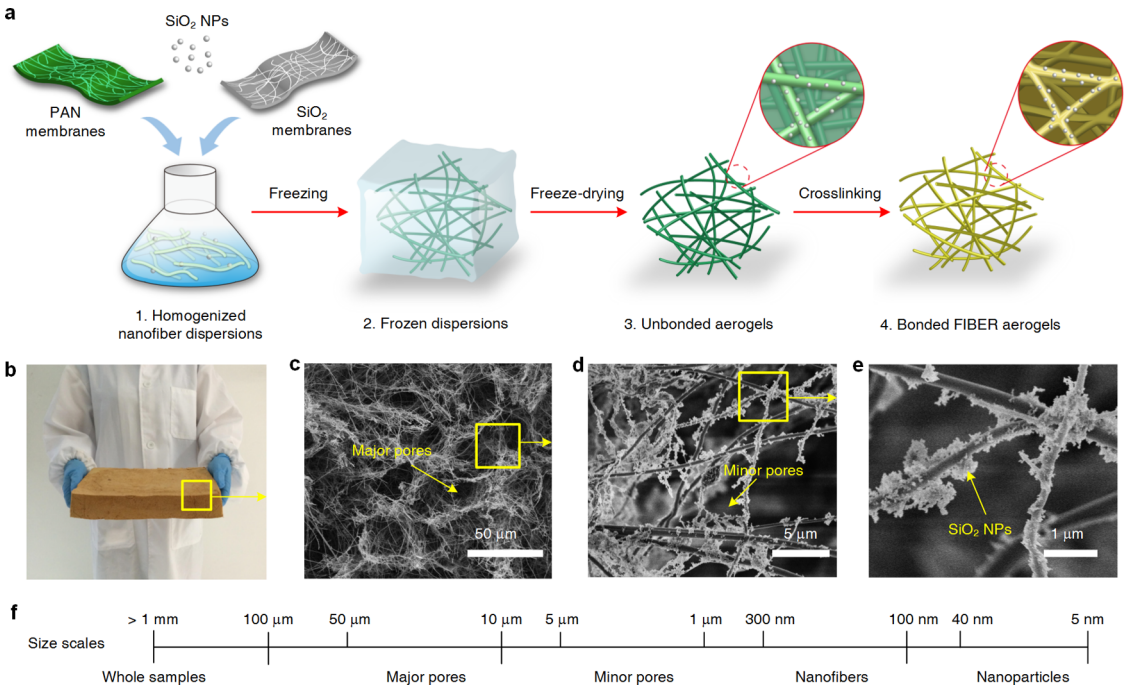

Figure 1. Design, processing, and cellular architectures of FIBER aerogels. (a) Schematic showing the synthetic steps. 1, Homogenized nanofiber dispersions are fabricated *via* high-speed homogenization. 2, Frozen dispersions are prepared by freezing in ice−water bath. 3, Unbonded aerogels are prepared by freeze-drying nanofiber dispersions. 4, The resultant bonded FIBER aerogels are prepared by the cross-linking treatment. (b) An optical image of a FIBER aerogel on a large scale of 2.5 L. (c−e) Microscopic architecture of FIBER aerogels at various magnifications, showing the hierarchical cellular fibrous structure. (f) Schematic representation of the scales of relevant structures. The FIBER aerogels were prepared in the case of a SiO_2 NPs concentration of 0.5 wt %.

Compared with the traditional sol−gel method for preparing aerogels,[11,12] our synthesis methodology combined the simplicity of the gelation-free assembly process and the large-scale availability of electrospun nanofibers. The synthesis can be completed within a day, even on a multiliter scale (Figure 1b and Figure S8); the resulting FIBER aerogels can be formed in any shape desired, such as cylinder, triangular prism, pentagonal prism, cuboid, and cone (Figure S9). The density of the as-prepared FIBER aerogels (SiO_2 NPs concentration of 0.5 wt %, see the data of other concentrations in Table S1) was 17.80 ± 0.29 mg cm^{-3}, which corresponded to a porosity of 98.63 ± 0.20%, and almost belongs to the lowest reported values of emulsion separation materials.[8,17] Of particular interest is that the fibrous freeze-shaping also simultaneously induces the nanofibers to be organized in a unique cellular architecture. Figure 1c−e presents typical scanning electron microscope (SEM) images of the FIBER aerogels with a SiO_2 NPs concentration of 0.5 wt %. The FIBER aerogels exhibited an obvious open-cell geometry with a major cellular pore size of 10−50 μm (Figure 1c), and these cells were highly interconnected by numerous minor cellular pores with sizes of 1−5 μm (Figure 1d). The significant difference between FIBER aerogels and other cellular aerogels was their unique fibrous cell networks that consisted of bonded nanofibers, despite the diameter of nanofibers being ~50 times thinner than that of traditional polymeric foams (10−30 μm).[31] Moreover, zooming in on the single fibers revealed that the SiO_2 NPs were well-positioned on the surface of fibers, indicating the effective construction of nanoscale roughness in aerogels (Figure 1e). Figure 1f also contains scale bars showing all the relevant sizes within these hierarchical cellular structures. The formation principle of the hierarchical cellular structure could be attributed to the phase separation induced by the crystallization of camphene.[32,33] When a nanofiber dispersion was frozen, the nanofibers were rejected from the moving solidification front and accumulated between the growing cellular solvent crystals, which was governed by complex and dynamic liquid−fiber and fiber−fiber interactions. A simple model of formation mechanism is schematically presented in Figure S10.

In dramatic contrast to the brittle nature of traditional colloidal aerogels, the FIBER aerogels (taken the sample with the SiO_2 NPs concentration of 0.5 wt % as an example) exhibited outstanding mechanical properties for large deformations without fractures (insets in Figure 2a and Movie S1). Stress−strain ($\sigma-\varepsilon$) behavior observed from Figure 2a showed a highly nonlinear and closed hysteresis, which are typical of viscoelastic, energy-dissipative, and highly deformable materials, for example, rubber.[34] Two distinct stages were observed during the loading process:[32,35] a linear elastic regime at $\varepsilon < 60\%$, corresponding to the bending and elastic buckling of cell walls; and an abrupt

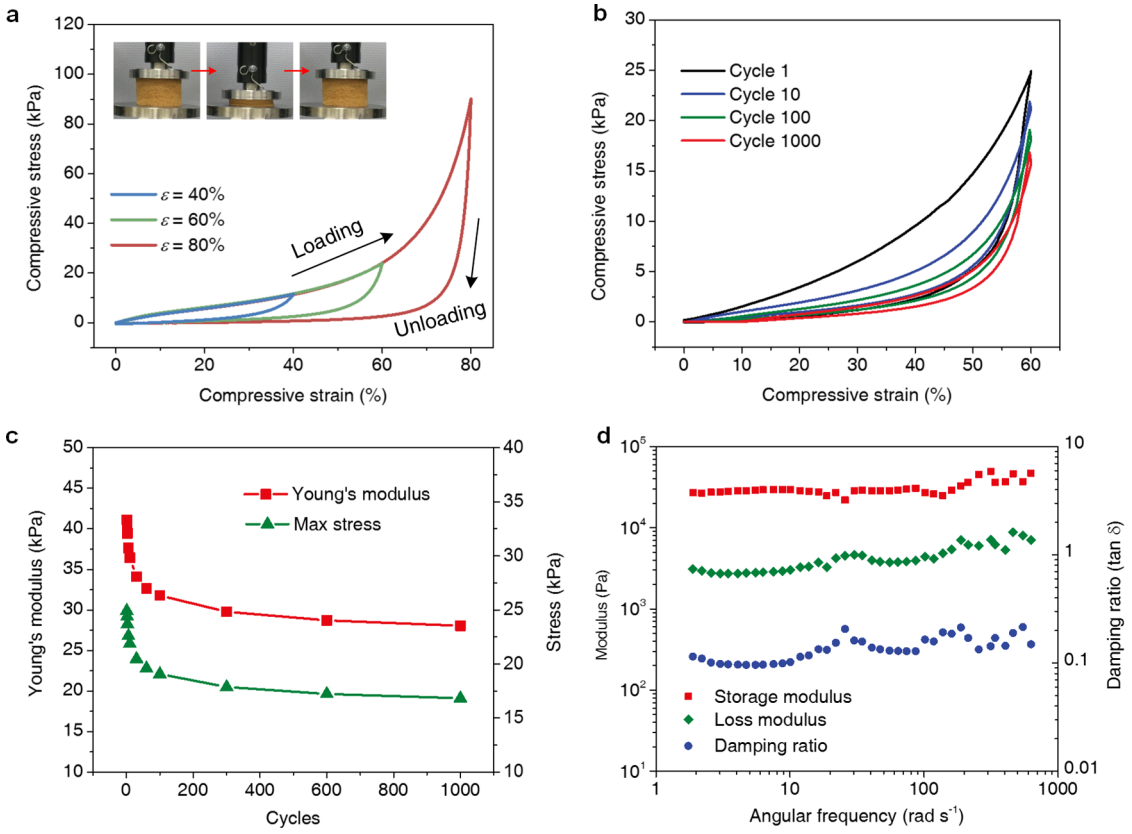

Figure 2. Multicycle compression test results of FIBER aerogels. (a) Compressive stress *versus* strain curves for FIBER aerogels along the loading direction. Insets: Photographs of the FIBER aerogels under a compressing and releasing cycle (ε = 80%). (b) $\sigma-\varepsilon$ curves of several selected cycles on a FIBER aerogel during repeated compressions (the first, 10th, 100th, and 1000th cycle). (c) History of Young's modulus and maximum stress as a function of the test cycles. (d) Dynamic rheological behavior of FIBER aerogels (oscillatory strain of $\pm$3%). The FIBER aerogels were prepared in the case of a SiO_2 NPs concentration of 0.5 wt %.

stress increasing regime, corresponding to densification of cells. The maximum stress was 24.1 kPa for the first elastic regime and 90.2 kPa at 80% strain; these values were significantly higher than those of other aerogels with similar densities.[36,37]

The highly elastic FIBER aerogels also exhibited excellent cycling performance. Hysteresis curves for 1000 loading−unloading fatigue cycles at a large ε of 60% (Figure 2b) showed slight plastic deformations (2.4% at 100th, 8.3% at 1000th) for FIBER aerogels; they still retained over 65% of the original Young's modulus and maximum stress (Figure 2c), highlighting the structural robustness. In comparison, a plastic deformation of larger than 20% is typical for polymeric foams.[30] Moreover, the frequency dependence of the storage modulus (E') and loss modulus (E'') presented in Figure 2d revealed that the E' and E'' were nearly stable and were independent of the angular frequency (ω) ranging from 1.8 to 628 rad s^{-1}. A small damping ratio of 0.1−0.25 indicated that the elastic response was predominant and that the FIBER aerogels contained strong, viscoelastic fibrous networks.[35,37] In addition, the dynamic test also revealed that the FIBER aerogels recovered their original shape at extremely high speed of 1440 mm min^{-1} (ω = 628 rad s^{-1}), which was 114% higher than those of conventional polymeric and carbon foams (~672 mm min^{-1}).[35,36]

The micro- and nanoscale composite structure is crucial for obtaining superwetting behavior according to the Cassie model.[2,17] On the basis of this principle, the hierarchical porous structure of FIBER aerogels was controlled by changing the concentration of SiO_2 NPs in precursor dispersions from 0.01 to 2 wt %. As shown in Figure 3a and Figure S11, by inclusion of SiO_2 NPs, the morphologies of the resultant aerogels were remarkably changed by creating nanoscaled rough structures on the surface of nanofibers. With increasing SiO_2 NPs concentrations, the average pore size of aerogels quickly decreased from 18.9 to 4.2 μm, meanwhile, the specific surface area (SSA) of aerogels increased dramatically from 2.66 to 76.54 m^2 g^{-1} (Figure 3b, Figure S12, and Table S1). This hierarchical rough structure significantly reduced the water−solid contact area, finally enhanced the wettability of aerogels. As shown in Figure 3c, the aerogels prepared from pure fiber dispersions exhibited a comparable hydrophobicity with a water contact angle (WCA) of 138°, which was attributed to the low surface energy of PBZ coating layer on fiber surface. With the addition of SiO_2 NPs to 2 wt %, a noteworthy increase of WCA

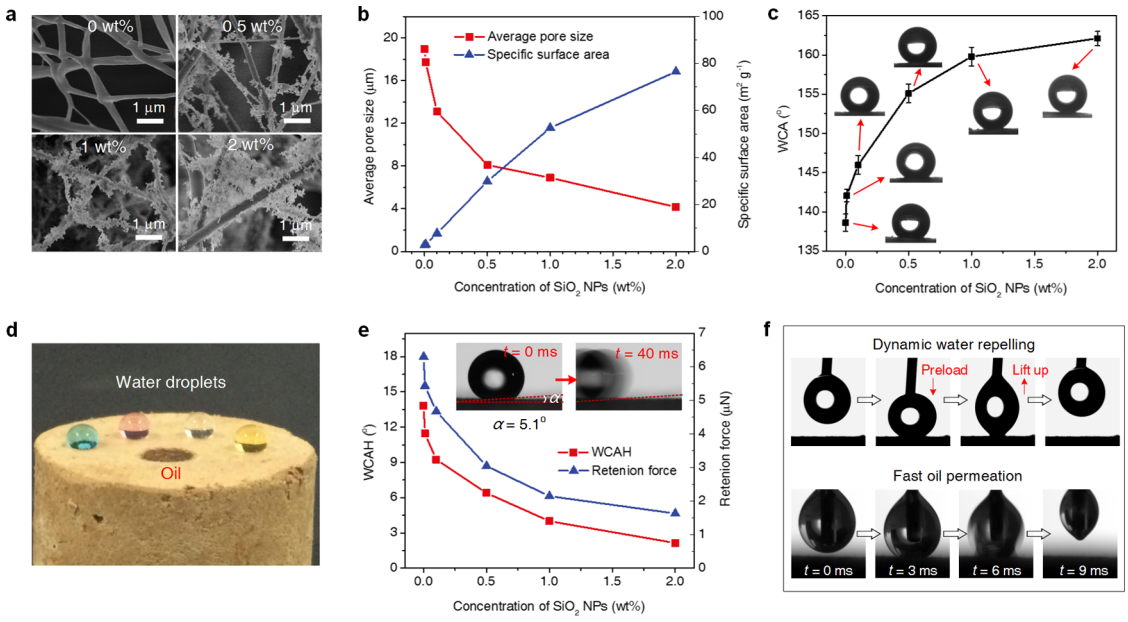

Figure 3. Characterization of microstructure and wettability of FIBER aerogels. (a) SEM images of FIBER aerogels with the SiO_2 NPs concentrations of 0, 0.5, 1, and 2 wt %. (b) Variation of the average pore size and SSA of the FIBER aerogels with increasing SiO_2 NPs concentrations. (c) Variation of the WCA of the FIBER aerogels with increasing SiO_2 NPs concentrations. (d) Droplets of dyed water and oil on the top of a FIBER aerogel. (e) The WCAH and retention force as a function of SiO_2 NPs concentrations, insets show a water droplet (10 μL) sliding at a low angle of 5.1° on the surface of the FIBER aerogel (2 wt % SiO_2 NPs). (f) Photographs of dynamic measurements of water adhesion (top) and oil permeation (bottom) on the surface of the FIBER aerogel (2 wt % SiO_2 NPs).

to 162° could be observed, confirming the superhydrophobicity of FIBER aerogels. This is because more air is trapped underneath the water droplet as a cushion on the surface of the FIBER aerogels.[3] Significantly, all the FIBER aerogels exhibited prominent superoleophilicity with the extremely low oil contact angle (OCA) of 0° (Figure 3d) because of the oleophilicity of PBZ that contains numerous benzene groups.[25,38]

Other very significant wetting properties to study contact behavior are water contact angle hysteresis (WCAH) and sliding angle (SA), which directly characterize the resistance to water mobility. As demonstrated in Figure 3e, the WCAH decreased with increasing SiO_2 NPs concentrations, achieving the lowest value of 2.2° for the aerogels with 2 wt % SiO_2 NPs. This low value of hysteresis indicated that the water could not penetrate into the aerogels at large extent and sat on the asperities of the surface with the minimum liquid solid adhesion; thus the water droplets could roll off the surface easily with a minute SA of 5.1°, as shown in the insets of Figure 3e. On the basis of the relevant measured WCAH values and droplet volume (10 μL), the estimated liquid retention forces of the FIBER aerogels ranged from 6.29 to 1.63 μN,[39] which were better than those of the state-of-the-art lotus-leaf-inspired hydrophobic surfaces, whose liquid retention forces are of the order of 10 μN at similar liquid volume.[17] To examine the dynamic wetting behavior of water on the FIBER aerogels, a high-speed camera system was used to record the adhesion and permeating process of a liquid droplet. Figure 3f (top) showed the photographs of a water droplet (3 μL) touching and leaving the aerogel surface. The droplet was forced to sufficiently contact the aerogel surface with an obvious deformation, and it was then lifted up. The corresponding photographs of the water droplet showed almost no deformation when leaving the aerogel surface, thus confirming the extremely low water adhesion for aerogels. Simultaneously, the aerogels behaved as a superior oil-adhesion property. As demonstrated in Figure 3f (bottom), when a 3 μL oil droplet (petroleum ether) contacted the aerogel surface, it spread out quickly and a nearly zero contact angle was achieved. The whole process was complete within 6 ms, suggesting the prominent property of aerogels for oil wetting. In addition, the FIBER aerogels still exhibited the robust superhydrophobicity after being immersed in oil with an underoil WCA of >150° (see Figure S13 and Supporting Information Discussions), which could be explained that the trapped air in the pores of aerogels was equally substituted by immiscible oil.[3] This promising superhydrophobic and superoleophilic wettability ensures fast oil permeation and moving through the aerogels and avoids direct contact between water and aerogels during oil/water separation, which could greatly enhance the separation performance of the aerogels and keep separation efficiency stable with time.[2,7]

To test the separation capability of the FIBER aerogels, a surfactant-stabilized water-in-oil (petroleum ether) emulsion was prepared using span 80 (0.1 wt %) with a 1 wt % water concentration (see details in Figure S14—16

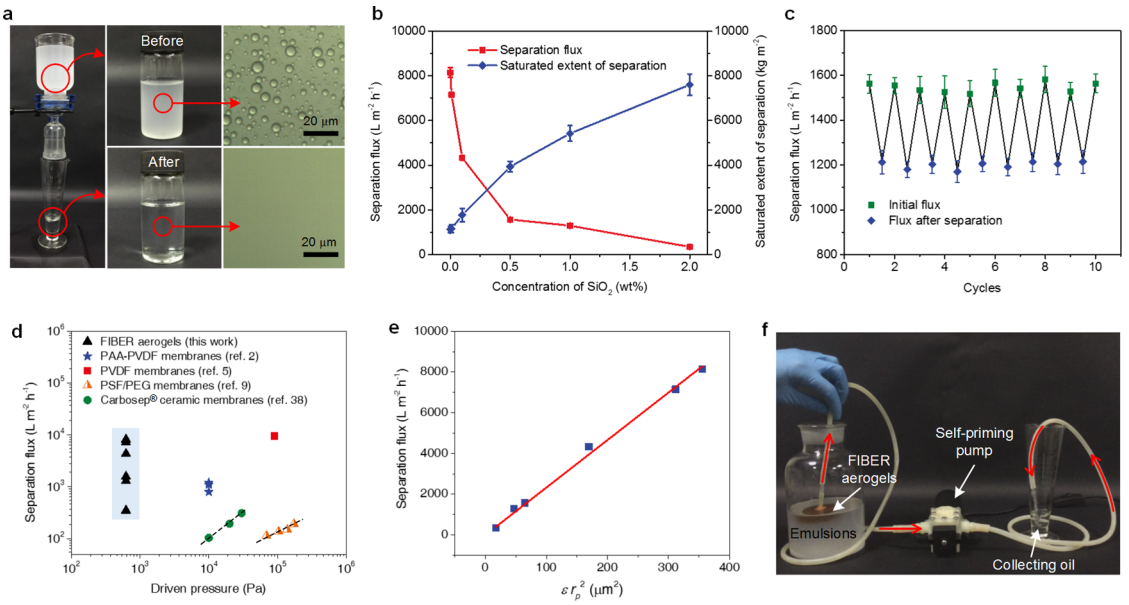

Figure 4. Separation of water-in-oil emulsions using FIBER aerogels. (a) Separation apparatus with the facile gravity-driven separation of water-in-oil emulsions using the FIBER aerogels and the microscopic images of emulsions before and after separation. (b) Separation flux and saturated extent of separation of FIBER aerogels with increasing SiO_2 NPs concentrations. (c) Change of the flux and flux recovery over 10 cycles (the sample with 0.5 wt % SiO_2 NPs was taken as an example). (d) The relative separation flux and driven-pressure of selected separation materials. (e) The separation flux as a function of εr_p^2 refer to the Hagen−Poiseuille law. (f) Photograph of the oil collection apparatus continuously collecting pure oil from water-in-oil emulsions.

and Supporting Information Discussions). The water droplet size distribution (Figure S16) indicated that the greatest number fraction of droplet diameters was in the range of 2−10 μm. As shown in Figure 4a, the cylindrical FIBER aerogels (taken the sample with 0.5 wt % SiO_2 NPs as an example) with diameter of 40 mm and thickness of 5 mm were sandwiched between two vertical glass tubes, and the as-prepared emulsions were then poured onto FIBER aerogels to carry out filtration separation driven solely by gravity. Oil immediately permeated through the aerogels and meanwhile, emulsion droplets demulsified once touching the FIBER aerogels and water was retained above (see Movie S2). The optical microscopic images of collected filtrate showed that no droplet was observed in the whole image. Moreover, the oil purity was further determined by measuring the water weight percentage in the filtrate using a Karl Fischer analyzer. The collected filtrate exhibited an extremely low water content of less than 50 ppm, corresponding to a prominent purity over 99.995%, indicating an extremely high separation efficiency. This high qualified collected oil can satisfy the requirement of purity in the majority of industrial applications.[4,18] It is worth noting that all the micrometer-sized water droplets can be effectively separated even the sizes of droplets are smaller than the pore size of FIBER aerogels. This phenomenon can be explained that the separation process for the FIBER aerogels is on the basis of the coalescence separation rather than the size-sieving surface filtration, which intercepts the emulsified droplets by the coalescence of droplets in the numerous tortuous microchannels;[40−42] thus, the FIBER aerogels are expected to achieve higher separation fluxes under low driven-pressure.

The gravity-driven separation fluxes of emulsions permeating through the FIBER aerogels were obtained by calculating the flow volume in 1 min from the valid area of the aerogels (the volume of the feed solution was kept constantly at 200 mL), as demonstrated in Figure 4b. The FIBER aerogels without SiO_2 NPs exhibited a surprisingly high flux of 8140 ± 220 L m^{-2} h^{-1}. However, in that case the flux quickly decreased upon the running time, with a small saturated extent of 1132 ± 140 kg m^{-2}. As discussed above, the coalesced water droplets accumulated over time and would eventually reverse the surface wettability of channels from hydrophobic to hydrophilic, finally blocking the oil transportation paths.[2,40] With increasing SiO_2 NPs contents in FIBER aerogels, the separation flux gradually decreased, whereas the flux became more stable upon running time. The FIBER aerogels with 2 wt % SiO_2 NPs contents exhibited a comparable flux of 350 ± 45 L m^{-2} h^{-1} but a promising saturated extent of 7612 ± 480 kg m^{-2}. In consideration the ultralight feature of the FIBER aerogels (<30 mg cm^{-3}), the saturated extent per gram of FIBER aerogels increased from 16.4 to 50.7 kg g^{-1} with the increase of SiO_2 NPs contents (Figure S17), indicating that the FIBER aerogels can separate over 15 000 times of their weight of emulsions, which has rarely been found in other porous separation materials.[12] Moreover, these

separation fluxes are comparable to those of reported membranes used with an external applied pressure,[2,6,10,46] as shown in Figure 4d. Considering that the separation was driven solely by gravity, such separation performance is very promising from the viewpoint of energy conservation, in contrast to the traditional filtration membranes such as UF membranes where a driven-pressure of more than 10^5 Pa is usually applied to accomplish emulsion separation. In addition, the antifouling performance of FIBER aerogels (taken the sample with 0.5 wt % SiO_2 NPs as an example) was performed as displayed in Figure 4c. For each cycle, the FIBER aerogels continuously separated a certain amount of oil (1000 kg m^{-2}) and then the aerogels were simply rinsed with ethanol to recover the flux. It can be seen that the flux exhibited a slight decrease within one cycle, then it recovered completely to the starting flux after ethanol washing, which could be attributed to the good stability of the well-bonded nanofibrous structure during cycle separation (see details in Figure S18 and Supporting Information Discussion). These results indicate an excellent antifouling property of the FIBER aerogels for long-term use.

To provide an insight into the mechanism of oil permeation, the Hagen−Poiseuille equation ($J = \varepsilon r_p^2 \Delta P/8\mu L\tau$) was used to analyze the flux of oil through the FIBER aerogels.[43−45] In this equation, the flux J is described as a function of the porosity ε, the pore radius r_p, the pressure drop ΔP, the liquid viscosity μ, the thickness L, and the tortuosity τ (that is, the ratio of the total distance traveled by the oil to L). In our experimental condition, the ΔP (fixed gravity pressure of 625 Pa), μ of petroleum ether (0.3×10^{-3} Pa s), and the L (5 mm) can be considered as unchanged parameters. Flux is thus only correlated to ε, r_p, and τ. As observed from Figure 4e, the flux (J) increased linearly with the relevant porous parameters (εr_p^2), revealing that the tortuosity of FIBER aerogels was nearly stable and was independent of the SiO_2 NPs concentrations. The calculated tortuosities for various FIBER aerogels were in the range of 21−28 (Table S1), which were about 1 order of magnitude higher than that of conventional UF membranes (<1.5).[8,43] These high tortuosities indicated that the real permeation path of emulsions was significantly longer than the thickness of the aerogels; thus, the emulsified water droplets were easy to be coalesced in these long tortuous channels, resulting in the high separation efficiency.

To further predict the separation flux of FIBER aerogels under different driven-pressure, we proposed the $J = k\Delta P$ scaling law for the separation of oil/water emulsion by using FIBER aerogels. The coefficient k ($k = \varepsilon r_p^2/8\mu L\tau$) were calculated to be 13.03, 11.44, 6.92, 2.52, 2.07, and 0.56 for FIBER aerogels with SiO_2 NPs concentrations of 0, 0.01, 0.1, 0.5, 1, and 2 wt %, indicating that the fluxes of FIBER aerogels with low SiO_2 NPs concentrations were more sensitive to the driven-pressure. On the basis of these theoretical analysis, more parameters have been checked to evaluate the separation performance of FIBER aerogels, including the types of oil phase (gasoline and diesel) and separation-driven pressure. The relevant measured separation fluxes matched well with the theoretical values (Figure S19, Figure S20, and Supporting Information Discussion), conforming the good usability of the FIBER aerogels toward various conditions. Furthermore, the mechanically robust FIBER aerogels achieved the collection of pure oil from the oil/water emulsions *via* a novel, continuous, and convenient pumping method. As demonstrated in Figure 4f, only the pure oil was absorbed by the FIBER aerogels and flows along the pipes to the collecting cup, leaving the FIBER aerogels consistently able to collect the oil (see detail in Movie S3 and Supporting Information Discussion). This novel pumping technique makes the separation of oil/water emulsions easier and faster, which can bring FIBER aerogels a step closer to practical applications.

CONCLUSIONS

In conclusion, we have demonstrated a gelation-free, synergistic assembly strategy for the fabrication of hierarchical cellular structured FIBER aerogels through the combination of electrospun nanofibers and the fibrous freeze-shaping method. With superelasticity, superhydrophobic-superoleophilic wettability, and high pore tortuosity, the FIBER aerogels can effectively separate water-in-oil emulsions driven solely by gravity, with high separation efficiency and higher fluxes than traditional filtration membranes with pressure-driven. More importantly, the FIBER aerogels exhibit a superior antifouling property, ease to cycle, and good usability, which match well with the requirements for treating the real emulsions on a massive scale. We anticipate that our FIBER aerogels will have numerous applications, including the cleanup of oil spills, wastewater treatment, fuel purification, and the separation of commercially relevant emulsions.

EXPERIMENTAL METHODS

Preparation of PAN and SiO_2 Nanofibers. For PAN nanofibers, the precursor solution was prepared by dissolving PAN (M_n = 90000, Spectrum) in dimethylformamide at a concentration of 6 wt %. The electrospinning was performed using a DXES-3 spinning machine (Shanghai Oriental Flying Nanotechnology Co., Ltd., China). The solution was loaded into a syringe capped with a 6-G metal needle with a controllable feed rate of 2 mL h^{-1}. A high voltage of 20 kV was applied to the needle tip, resulting in the generation of a continuous jetting stream. The resultant PAN nanofiber membranes were deposited on the aluminum

foil-covered grounded metallic rotating roller (rotating rate was 50 rpm) at a 15 cm tip-to-collector distance. In the case of SiO_2 nanofibers, the precursor solution was prepared by dissolving poly(vinyl alcohol) (PVA, M_n = 86 000, Wako) in pure water at 80 °C with vigorous stirring. A silica precursor solution with a molar composition of tetraethyl orthosilicate (TEOS):H_3PO_4:H_2O = 1:0.01:11 was prepared *via* hydrolysis and polycondensation by dropwise addition of H_3PO_4 for 12 h. The resultant silica precursor solution was added to the PVA solution (weight ratio of 1:1) and stirred for another 4 h. Following, the electrospinning was performed under an applied voltage of 18 kV and at a controllable feed rate of 1 mL h^{-1}. The resultant hybrid nanofibers were deposited onto the aluminum foil-covered grounded metallic rotating roller with a rotation rate of 50 rpm at a 20 cm tip-to-collector distance. To obtain pure SiO_2 nanofibers, the as-spun nanofibers were calcined at 800 °C in air by gradually increasing the temperature at a heating rate of 5 °C min^{-1} to remove the PVA. The relevant temperature and humidity during electrospinning were 25 °C and 50%. The FE-SEM images and diameter analysis of these two types of nanofibers were demonstrated in Figure S1.

Fabrication of FIBER Aerogels. BAF-a monomers were synthesized using bisphenol AF, amine, and paraformaldehyde *via* the Mannich reaction, as described previously with minor modifications (see details in Figure S2a and Supporting Information Methods). In a typical experiment for the synthesis of FIBER aerogels with SiO_2 NPs concentrations of 0.5 wt % (see details in Figure S3, Figure S4, and Supporting Information Methods), 0.8 g of PAN and 0.2 g of SiO_2 nanofiber membranes were cut into 1 × 1 cm^2 pieces, and were dispersed in 100 mL of camphene at 70 °C by homogenizing the mixture for 30 min at 13 000 rpm using a high-speed homogenizer (SDF400, Qile Tech Co., Ltd., China), yielding uniform nanofiber dispersions with an average fiber length of 50 μm. Subsequently, the 0.5 g of SiO_2 NPs (diameters of 7−40 nm) and 0.5 g of BAF-a were added to the dispersion with further stirring for 20 min. The obtained dispersions were poured into the desired mold, frozen in ice−water bath, and then freeze-dried (Labconco FreeZone freeze-drying system) for 24 h to obtain the unbonded aerogels. Finally, they were heated at 240 °C for 1 h in air, giving rise to the bonded FIBER aerogels. Other FIBER aerogels with different SiO_2 contents were fabricated by adjusting the concentrations of SiO_2 NPs in dispersions.

Mechanical Properties Measurements. The compression tests were performed using Instron 3365 testing system (Instron Co., Ltd., USA) equipped with two flat-surface compression stages and 1000-N load cells. Cylindrical FIBER NFA samples with diameters of ∼30 mm were used. The $\sigma-\varepsilon$ curves with ε = 40, 60 and 80% were measured at a strain rate of 30 mm min^{-1}, and a 3% prestrain was applied to make a uniform flat contact between the compression heads and the sample and to prevent slipping of the sample. A 1000-cycle loading−unloading fatigue cyclic test was performed by measuring σ *versus* ε = 60% at a strain rate of 300 mm min^{-1} with a 3% prestrain. Dynamic compressive viscoelastic measurements of the FIBER aerogels were performed using a TA-Q800 DMA instrument with a parallel-plate compression clamp; the gap distance between the two plates was fixed at 4 mm. E' and E'' as a function of ω from 1.8 to 628 rad s^{-1} were measured with an oscillatory strain of ±3% and a prestrain of 5%.

Emulsion Separation Experiments. To preparing the water-in-oil emulsions, the surfactant (0.1 wt %) was first dissolved in oil, and a certain amount of water (1 wt %) was added into the oil. Following, the mixture was emulsified by a high-speed homogenizer (5000 rpm for 5 min) and was further homogenized by an ultrasonic treatment (5 min), as shown in Figure S14. The thermodynamic stability of as-prepared emulsions was demonstrated in Figure S15 and Supporting Information Discussions. The cylindrical FIBER aerogels (taken the sample with 0.5 wt % SiO_2 NPs as an example) with diameter of 40 mm and thickness of 5 mm were sandwiched between two vertical glass tubes. The freshly prepared emulsion was poured onto the samples and the oil spontaneously permeated. The flux was determined by calculating the volume of oil permeated within 1 min. The regulation of separation-driven pressure was achieved by changing the height of emulsions, as shown in Figure S19.

Characterization. The weights of the FIBER aerogels were determined using a Mettler Toledo Micro balance (AT-20) with a readability of 2 μg. The density (apparent density) of the FIBER aerogels was measured on the basis of the ISO 845:2006 standard, which was calculated by the weight of solid contents without including the weight of air entrapped in pores. As the samples were weighted in air, the weight of air was automatically eliminated. The porosity and compression work of FIBER aerogels was determined based on the standard practice for cellular materials, as demonstrated in the Supporting Information Methods. The SEM images were examined using a Hitachi S4800 field-emission SEM system. FT-IR spectra were collected with a Nicolet 8700 spectrometer in the range 4000−400 cm^{-1}. DSC measurements were performed with a TA-Q200 differential scanning calorimeter. The pore size and distribution were measured using an air poremeter (MMN-1200A, Porous Materials Co., Ltd., USA) based on capillary flow analysis method (see details in Supporting Information Methods). N_2 adsorption−desorption isotherms and BET SSA were examined at 77 K by an ASAP 2020 physisorption analyzer (Micromeritics Co., USA). WCA (3 μL), OCA (3 μL), and SA (10 μL) measurements were performed by a contact angle goniometer Kino SL200B equipped with tilting base. The water contact angle hysteresis was measured using increment decrement method.

Conflict of Interest: The authors declare no competing financial interest.

Acknowledgment. This work is supported by the National Natural Science Foundation of China (No. U1232116 and 51322304), the Fundamental Research Funds for the Central Universities, and the "DHU Distinguished Young Professor Program".

Supporting Information Available: Synthetic route of BAF-a monomers, SEM images of dispersed nanofibers, FT-IR and DSC results, volume shrinkage results, optical images of FIBER aerogels with large scale and diverse shapes, formation mechanism of the hierarchical cellular structure, SEM images of FIBER aerogels with the SiO_2 NPs contents, thermodynamically stability of emulsions, water droplet size distribution of the water-in-oil emulsions, separation performance under different driven pressure, and structure changes during the cycle separation. This material is available free of charge *via* the Internet at http://pubs.acs.org.

REFERENCES AND NOTES

1. Kota, A. K.; Kwon, G.; Choi, W.; Mabry, J. M.; Tuteja, A. Hygro-Responsive Membranes for Effective Oil−Water Separation. *Nat. Commun.* **2012**, *3*, 1025.
2. Zhang, W.; Zhu, Y.; Liu, X.; Wang, D.; Li, J.; Jiang, L.; Jin, J. Salt-Induced Fabrication of Superhydrophilic and Underwater Superoleophobic PAA-g-PVDF Membranes for Effective Separation of Oil-in-Water Emulsions. *Angew. Chem., Int. Ed.* **2014**, *53*, 856–860.
3. Zhang, J.; Seeger, S. Polyester Materials with Superwetting Silicone Nanofilaments for Oil/Water Separation and Selective Oil Absorption. *Adv. Funct. Mater.* **2011**, *21*, 4699–4704.
4. Kwon, G.; Kota, A. K.; Li, Y.; Sohani, A.; Mabry, J. M.; Tuteja, A. On-Demand Separation of Oil−Water Mixtures. *Adv. Mater.* **2012**, *24*, 3666–3671.
5. Zhang, F.; Zhang, W. B.; Shi, Z.; Wang, D.; Jin, J.; Jiang, L. Nanowire-Haired Inorganic Membranes with Superhydrophilicity and Underwater Ultralow Adhesive Superoleophobicity for High-Efficiency Oil/Water Separation. *Adv. Mater.* **2013**, *25*, 4192–4198.
6. Tao, M.; Xue, L.; Liu, F.; Jiang, L. An Intelligent Superwetting PVDF Membrane Showing Switchable Transport Performance for Oil/Water Separation. *Adv. Mater.* **2014**, *26*, 2943–2948.
7. Zhang, W.; Shi, Z.; Zhang, F.; Liu, X.; Jin, J.; Jiang, L. Superhydrophobic and Superoleophilic PVDF Membranes for

Effective Separation of Water-in-Oil Emulsions with High Flux. *Adv. Mater.* **2013**, *25*, 2071–2076.
8. Shi, Z.; Zhang, W.; Zhang, F.; Liu, X.; Wang, D.; Jin, J.; Jiang, L. Ultrafast Separation of Emulsified Oil/Water Mixtures by Ultrathin Free-Standing Single-Walled Carbon Nanotube Network Films. *Adv. Mater.* **2013**, *25*, 2422–2427.
9. Li, Y. P.; Xiao, W. W.; Xiao, K.; Berti, L.; Luo, J. T.; Tseng, H. P.; Fung, G.; Lam, K. S. Well-Defined, Reversible Boronate Crosslinked Nanocarriers for Targeted Drug Delivery in Response to Acidic pH Values and *cis*-Diols. *Angew. Chem., Int. Ed.* **2012**, *51*, 2864–2869.
10. Chakrabarty, B.; Ghoshal, A. K.; Purkait, M. K. Ultrafiltration of Stable Oil-in-Water Emulsion by Polysulfone Membrane. *J. Membr. Sci.* **2008**, *325*, 427–437.
11. Pierre, A. C.; Pajonk, G. M. Chemisty of Aerogels and Their Applications. *Chem. Rev.* **2002**, *102*, 4243–4265.
12. Hüsing, N.; Schubert, U. Aerogels—Airy Materials: Chemisty, Structure, and Properties. *Angew. Chem., Int. Ed.* **1998**, *37*, 22–45.
13. Sun, H.; Xu, Z.; Gao, C. Multifunctional, Ultra-Flyweight, Synergistically Assembled Carbon Aerogels. *Adv. Mater.* **2013**, *25*, 2554–2560.
14. Chen, N.; Pan, Q. M. Versatile Fabrication of Ultralight Magnetic Foams and Application for Oil−Water Separation. *ACS Nano* **2013**, *7*, 6875–6883.
15. Li, L.; Xiang, S. L.; Cao, S. Q.; Zhang, J. Y.; Ouyang, G. F.; Chen, L. P.; Su, C. Y. A Synthetic Route to Ultralight Hierarchically Micro/Mesoporous Al(III)-Carboxylate Metal-Organic Aerogels. *Nat. Commun.* **2013**, *4*, 1774.
16. Li, Y. Q.; Samad, Y. A.; Polychronopoulou, K.; Alhassan, S. M.; Liao, K. Carbon Aerogel from Winter Melon for Highly Efficient and Recyclable Oils and Organic Solvents Absorption. *ACS Sustainable Chem. Eng.* **2014**, *2*, 1492–1497.
17. Wang, X.; Ding, B.; Yu, J.; Wang, M. Engineering Biomimetic Superhydrophobic Surfaces of Electrospun Nanomaterials. *Nano Today* **2011**, *6*, 510–530.
18. Gao, X.; Xu, L. P.; Xue, Z.; Feng, L.; Peng, J.; Wen, Y.; Wang, S.; Zhang, X. Dual-Scaled Porous Nitrocellulose Membranes with Underwater Superoleophobicity for Highly Efficient Oil/Water Separation. *Adv. Mater.* **2014**, *26*, 1771–1775.
19. Zhu, H. G.; Chen, D. Y.; Li, N. J.; Xu, Q. F.; Li, H.; He, J. H.; Lu, J. M. Graphene Foam with Switchable Oil Wettability for Oil and Organic Solvents Recovery. *Adv. Funct. Mater.* **2015**, *25*, 597–605.
20. Chen, N.; Pan, Q. M. Versatile Fabrication of Ultralight Magnetic Foams and Application for Oil-Water Separation. *ACS Nano* **2013**, *8*, 6875–6883.
21. Wang, B.; Liang, W. X.; Guo, Z. G.; Liu, W. M. Biomimetic Super-Lyophobic and Super-Lyophilic Materials Applied for Oil-Water Separation a New Strategy beyond Nature. *Chem. Soc. Rev.* **2015**, *44*, 336–361.
22. Hsu, P. C.; Wang, S.; Wu, H.; Narasimhan, V. K.; Kong, D.; Ryoung Lee, H.; Cui, Y. Performance Enhancement of Metal Nanowire Transparent Conducting Electrodes by Mesoscale Metal Wires. *Nat. Commun.* **2013**, *4*, 2522.
23. Greiner, A.; Wendorff, J. H. Electrospinning: A Fascinating Method for the Preparation of Ultrathin Fibers. *Angew. Chem., Int. Ed.* **2007**, *46*, 5670–5703.
24. Xu, Z.; Zhang, Y.; Li, P. G.; Gao, C. Strong, Conductive, Lightweight, Neat Graphene Aerogel Fibers with Aligned Pores. *ACS Nano* **2012**, *6*, 7103–7113.
25. Wang, X.; Ding, B.; Sun, G.; Wang, M.; Yu, J. Electro-Spinning/Netting: A Strategy for the Fabrication of Three-Dimensional Polymer Nano-Fiber/Nets. *Prog. Mater. Sci.* **2013**, *58*, 1173–1243.
26. Liu, J.; Yue, Z. R.; Fong, H. Continuous Nanoscale Carbon Fibers with Superior Mechanical Strength. *Small* **2009**, *5*, 536–542.
27. Ghosh, N. N.; Kiskan, B.; Yagci, Y. Polybenzoxazines—New High Performance Thermosetting Resins: Synthesis and Properties. *Prog. Polym. Sci.* **2007**, *32*, 1344–1391.
28. Yang, L.; Raza, A.; Si, Y.; Mao, X.; Shang, Y.; Ding, B.; Yu, J.; Al-Deyab, S. S. Synthesis of Superhydrophobic Silica Nanofibrous Membranes with Robust Thermal Stability and Flexibility *via in situ* Polymerization. *Nanoscale* **2012**, *4*, 6581–6587.
29. Si, Y.; Ren, T.; Li, Y.; Ding, B.; Yu, J. Fabrication of Magnetic Polybenzoxazine-based Carbon Nanofibers with Fe_3O_4 Inclusions with a Hierarchical Porous Structure for Water Treatment. *Carbon* **2012**, *50*, 5176–5185.
30. Mathur, R. B.; Dhami, T. L.; Bahl, O. P. Shrinkage Behavior of Modified PAN Precursors—Its Influence on the Properties of Resulting Carbon Fiber. *Polym. Degrad. Stab.* **1986**, *14*, 179–187.
31. Wang, X.; Feng, N.; Chang, S. Q. Effect of Precured Degrees on Morphology, Thermal, and Mechanical Properties of BR/SBR/NR Foams. *Polym. Compos.* **2013**, *34*, 849–859.
32. Qiu, L.; Liu, J. Z.; Chang, S. L. Y.; Wu, Y.; Li, D. Biomimetic Superelastic Graphene-based Cellular Monoliths. *Nat. Commun.* **2012**, *3*, 1241.
33. Deville, S. Freeze-Casting of Porous Ceramics: A Review of Current Achievements and Issues. *Adv. Eng. Mater.* **2008**, *10*, 155–169.
34. Xu, M.; Futaba, D. N.; Yamada, T.; Yumura, M.; Hata, K. Carbon Nanotubes with Temperature-Invariant Viscoelasticity from −196 to 1000 °C. *Science* **2010**, *330*, 1364–1368.
35. Kim, K. H.; Oh, Y.; Islam, M. F. Graphene Coating Makes Carbon Nanotube Aerogels Superelastic and Resistant to Fatigue. *Nat. Nanotechnol.* **2012**, *7*, 562–566.
36. Liang, H. W.; Guan, Q. F.; Chen, L. F.; Zhu, Z.; Zhang, W. J.; Yu, S. H. Macroscopic-Scale Template Synthesis of Robust Carbonaceous Nanofiber Hydrogels and Aerogels and Their Applications. *Angew. Chem., Int. Ed.* **2012**, *51*, 5101–5105.
37. Gibson, L. J.; Ashby, M. F. *Cellular Solids: Structure and Properties*; Cambridge University Press: Cambridge, U.K., 1999.
38. Li, B. Y.; Jiang, B. B.; Fauth, D. J.; Gray, M. L.; Pennline, H. W.; Richards, G. A. Innovative Nano-Layered Solid Sorbents for CO_2 Capture. *Chem. Commun.* **2011**, *47*, 1719–1721.
39. Wong, T. S.; Kang, S. H.; Tang, S. K. Y.; Smythe, E. J.; Hatton, B. D.; Grinthal, A.; Aizenberg, J. Bioinspired Self-Repairing Slippery Surfaces with Pressure-Stable Omniphobicity. *Nature* **2011**, *477*, 443–447.
40. Agarwal, S.; von Arnim, V.; Stegmaier, T.; Planck, H.; Agarwal, A. Role of Surface Wettability and Roughness in Emulsion Separation. *Sep. Purif. Technol.* **2013**, *107*, 19–25.
41. Oo, M. K. K.; Yang, Y. M.; Hu, Y.; Gomez, M.; Du, H.; Wang, H. J. Gold Nanoparticle-Enhanced and Size-Dependent Generation of Reactive Oxygen Species from Protoporphyrin IX. *ACS Nano* **2012**, *6*, 1939–1947.
42. Secerov Sokolovic, R. M.; Govedarica, D. D.; Sokolović, D. S. Separation of Oil-in-Water Emulsion Using Two Coalescers of Different Geometry. *J. Hazard. Mater.* **2010**, *175*, 1001–1006.
43. Karan, S.; Samitsu, S.; Peng, X. S.; Kurashima, K.; Ichinose, I. Ultrafast Viscous Permeation of Organic Solvents Through Diamond-Like Carbon Nanosheets. *Science* **2012**, *335*, 444–447.
44. Peng, X.; Jin, J.; Nakamura, Y.; Ohno, T.; Ichinose, I. Ultrafast Permeation of Water Through Protein-based Membranes. *Nat. Nanotechnol.* **2009**, *4*, 353–357.
45. Warkiani, M. E.; Bhagat, A. A. S.; Khoo, B. L.; Han, J.; Lim, C. T.; Gong, H. Q.; Fane, A. G. Isoporous Micro/Nanoengineered Membranes. *ACS Nano* **2013**, *7*, 1882–1904.
46. Lobo, A.; Cambiella, A.; Benito, J. M.; Pazos, C.; Coca, J. Ultrafiltration of Oil-in-Water Emulsions with Ceramic Membranes: Influence of pH and Crossflow Velocity. *J. Membr. Sci.* **2006**, *278*, 328–334.